

## Quasicrystalline low-friction coatings

J. M. DUBOIS, S. S. KANG, J. VON STEBUT

Laboratoire de Science et Génie des Matériaux Métalliques (CNRS UA 159), Ecole des Mines, Parc de Saurupt, F-54042 Nancy, France

Though expected on the grounds of fancying mathematics for one or two decades, real quasicrystalline alloys were discovered only five years ago [1]. These still partly mysterious materials have generated a considerable effort to understand their structure and investigate their fundamental properties [2]. The definition of atom positions within a lattice that is incompatible with the translational generative symmetry of conventional crystals is the focus of interest of many papers published so far. It is now best understood in the framework of the so-called high-dimensional crystallography [3]. Successful derivation of such positions from experimental data have been actually achieved for the icosahedral phase with point group symmetry  $m\bar{3}\bar{5}$  [4]. Elucidation of the decagonal phase [5], of point group symmetry  $10/mmm$ , is currently in progress.

The question of their formation and stability is of great fundamental importance but yet still obscure. A significant achievement was obtained with the report [6] that stable icosahedral-type crystals may be grown by a slow solidification technique. More recently, the discovery [7] of a supposedly perfectly stable icosahedral phase close to the composition  $Al_{64}Cu_{24}Fe_{12}$  launched a systematic investigation of the Al-Cu-3d metal systems. The  $Al_{64}Cu_{24}Fe_{12}$  alloy was found to grow single crystals with either dodecahedral or icosidodecahedral morphologies (Fig. 1a and b). The stable decagonal phase forms in Al-Cu-Co alloys [8] as well as in the vicinity of the composition  $Al_{66}Cu_{18}Fe_8Cr_8$ , growing characteristic needle-shaped deca-prismatic single crystals (Fig. 1c).

In fact, a careful study, using diffraction techniques, of the single crystals shown in Fig. 1 demonstrated that the actual structure is not truly quasicrystalline at room temperature. It is rather that of a crystalline material with a giant unit cell that very closely resembles the quasicrystalline phases. As a matter of fact, the  $Al_{64}Cu_{24}Fe_{12}$  alloy forms a rhombohedral crystal [9] (cell parameters:  $a = 3.22$  nm,  $\gamma = 36^\circ$ ) whereas the  $Al_{66}Cu_{18}Fe_8Cr_8$  one is orthorhombic [10] ( $a = 2.26$  nm,  $b = 1.23$  nm,  $c = 3.25$  nm). However, these crystalline, so-called approximant [11], phases transform reversibly into the corresponding true quasicrystals when heated up to the 650–750 °C temperature range [12].

Beside fundamental studies, interest has also been focused on the potential of applications of these new materials. Unfortunately, the first reports along these lines were rather negative. The  $T_2-Al_6Cu_3Li$  icosahedral phase was found too brittle to be of practical use [13]. The initiation and propagation of

cracks has been related to the presence of icosahedral crystals in stainless steel alloys [14]. Weakly ferromagnetic icosahedral phases have been discovered [15] but the moment carried by the magnetic atoms is too low so far to offer any hope of a commercial use of the alloy. This approach may lead, however, to some interesting breakthrough in the near future.

Taking advantage of the high hardness of quasicrystals, we have successfully improved the wear resistance of soft alloys such as aluminium-based alloys, copper or low-carbon steels. These metallic materials are often in use in an abrasive or erosive environment and suffer dramatically from severe wear conditions. Our study was based on a selection of two alloys which readily form quasicrystalline phases (or their approximant crystalline counterparts, see above) namely:

Alloy A of nominal composition  $Al_{65}Cu_{20}Fe_{15}$  (at%)

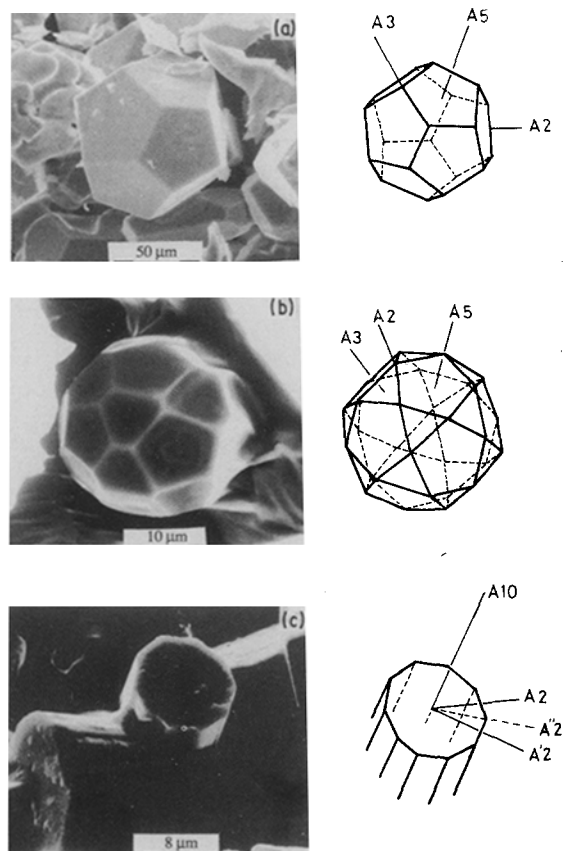


Figure 1 Single-crystal morphologies of the  $Al_{64}Cu_{24}Fe_{12}$  icosahedral phase, (a) pentagonal dodecahedron, and (b) icosidodecahedron; and (c) of the  $Al_{66}Cu_{18}Fe_8Cr_8$  decagonal phase (deca-prismatic crystal).

Alloy B of nominal composition  $\text{Al}_{64}\text{Cu}_{18}\text{Fe}_8\text{Cr}_8$  (at%)

Ingots of several kilograms were r.f. melted under an inert atmosphere (Ar or  $\text{N}_2$ ), starting from elemental constituents of purity better than 99.5%, and cooled back to room temperature at a speed of a few tens of degrees per second. In this as-cast state, the bulk ingots contain a mixture of several phases, one being the relevant non-crystallographic phase. Alloy A contained the approximant rhombohedral phase of the icosahedral phase, plus the monoclinic  $\theta\text{-Al}_{13}\text{Fe}_4$  compound [16], the  $\alpha\text{-Al}_3\text{Cu}_2$  phase [17] and in addition a newly discovered cubic phase (C) of approximate composition  $\text{Al}_7\text{Cu}_2\text{Fe}$  [12]. For the purpose of what follows, it is not necessary to distinguish any more between the icosahedral phase and the approximant crystal. Thus, we will refer to both of them as i-phase. The constituent phases of alloy A were identified by X-ray diffraction (Fig. 2a) and microprobe analysis which revealed that the amount of i-phase was about 50 vol%. The other alloy B contained the approximant to the decagonal phase (both denoted as d-phase hereafter), the previous crystalline phases the  $\beta\text{-Al}_7\text{Cu}_2\text{Fe}$  tetragonal phase [18] and a small amount of i-phase. The volume fraction of quasicrystalline phases was significantly increased by suitably long annealings at  $T = 840^\circ\text{C}$  (alloy A) or  $T = 730^\circ\text{C}$  (alloy B). The fraction of i-phase in alloy A then reached 85–90% (Fig. 2b) whereas alloy B was totally transformed into d-phase except for a very small amount of cubic phase (Fig. 2c).

Powders were then prepared by mechanical grinding of pieces of the annealed ingots to a mesh size in

the range 20 to 75  $\mu\text{m}$ . We used two techniques to coat the substrates, namely a supersonic jet gun that enables one to spray the melted powder at a speed as high as  $3600\text{ m s}^{-1}$  (Mach 12) and a more conventional  $\text{H}_2\text{-O}_2$  blowtorch designed for powder spraying. The mixture of  $\text{O}_2$  and  $\text{H}_2$  gases was overfed with hydrogen and the experimental set-up kept under a 70%  $\text{N}_2$ –30%  $\text{H}_2$  atmosphere in order to protect the coating as much as possible from oxidization. In the following, we shall refer to the spraying techniques by letters for the sake of brevity: S (supersonic gun) and T (blowtorch). Three types of alloy with particularly low hardness were chosen: (a) metallic copper, (b) AU4G and AU5GT aluminium-based alloys and (c) a commercial steel with low carbon content. The microhardness values of these materials (measured under a load of 30 g) are given in Table I. The surface of each substrate sample was prepared just before the coating deposition by sandblasting in order to clean it and increase its specific area. Coatings of varying thickness were obtained depending on the duration of the spray. The temperature of the substrate was controlled in the mean time but never raised above  $250^\circ\text{C}$ . After cooling back to room temperature, the upper surface was cleaned either by mechanical polishing or brushed so as to eliminate the powder particles that had not reacted with the coating underneath.

After being deposited, the sprayed powders are no longer pure quasicrystalline but rather a mixture of quasicrystals and crystalline phases. The i-phase is, however, easily detected by X-ray diffraction in coatings of alloy A (Fig. 3a). This mixture of phases is particularly stable as no change in the diffraction pattern is observed after annealing a specimen at  $400^\circ\text{C}$  for as long as 80 h. Alloy B coatings contain a significant amount of about 30 vol% of the i-phase (Fig. 3b) which is also most simply revealed in electron diffraction patterns (Fig. 4).

This i-phase, however, does not show the f.c.c. superlattice ordering characteristic of the Al–Cu–Fe icosahedral phase [7]. Instead, it is primitive and may be indexed with a six-dimensional lattice parameter  $a = 0.644\text{ nm}$  [19]. Other crystalline phases are a minute amount of cubic phase, hardly visible on the X-ray diffraction pattern (Fig. 3b) and a few volume per cent of  $\alpha\text{-Al}_2\text{O}_3$  oxide, the formation of which cannot be fully avoided with the blowtorch technique. Upon heating, this coating is slightly less stable than the previous one. Annealing it at  $530^\circ\text{C}$  for 30 h makes the icosahedral phase

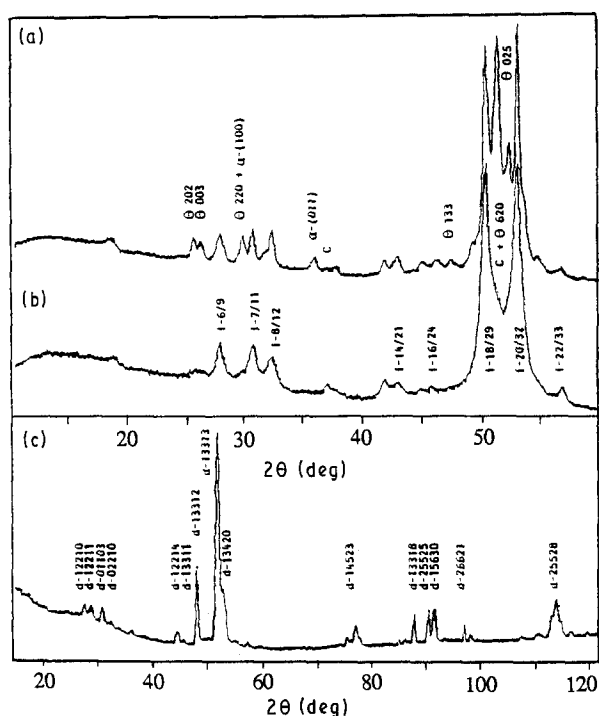


Figure 2 X-ray diffraction patterns for  $\lambda$  ( $\text{CoK}\alpha$ ) = 0.17889 nm of ingot A ( $\text{Al}_{65}\text{Cu}_{20}\text{Fe}_{15}$ ), (a) in the as-cast state and (b) after annealing; and (c) ingot B ( $\text{Al}_{66}\text{Cu}_{18}\text{Fe}_8\text{Cr}_8$ ) after annealing. Refer to [19] and [20] for the indexing of the i-phase pattern (b) and d-phase pattern (c), respectively.

TABLE I Substrates

Material	$H_V$	$\mu$ (indenter D, tip radius 0.2 mm)* $\pm 0.01$	$\mu$ (indenter B, tip radius 0.19 mm)* $\pm 0.01$
(a) copper	$48 \pm 5$	0.415 (80 N)	0.35 (80 N)
(b) AU4G	$87 \pm 15$	0.37 (60 N)	
AU5GT	$85 \pm 15$	0.435 (60 N)	
(c) steel	$120 \pm 30$	0.40 (80 N)	0.305 (80 N)

\* Load  $F_N$  is given in brackets. The accuracy of  $\pm 0.01$  is estimated from a set of at least three tests.

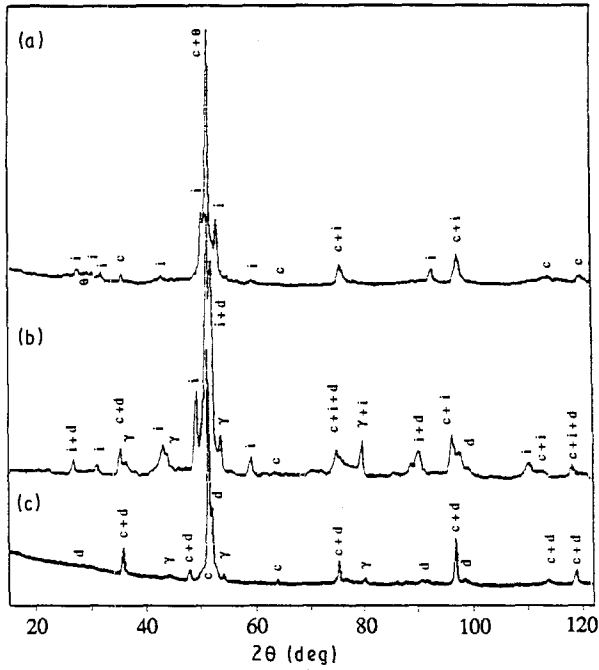


Figure 3 X-ray diffraction patterns ( $\lambda = 0.17889$  nm) of the coatings: (a) alloy A as-deposited, (b) = alloy B as-deposited and (c) after annealing at 530 °C for 30 h.

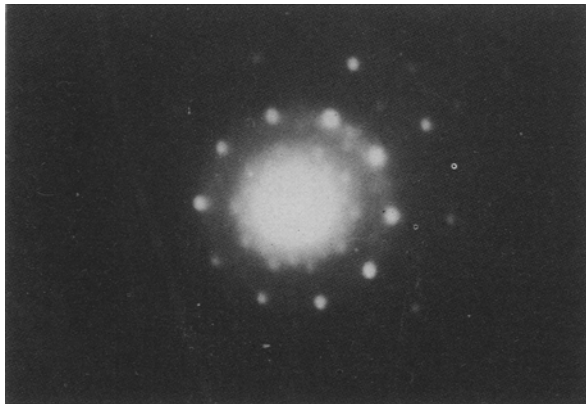


Figure 4 Electron diffraction pattern of a thin area in a coating with alloy B. The five-fold pattern is characteristic of the i-phase.

disappear (Fig. 3c). Conversely, the peaks of the d-phase show up as well as the amount of c-phase which has significantly increased. Note, however, that the coating does not transform at lower temperatures, thus being valuable for most purposes.

The microhardness is about the same for each composition and is considerably higher than that of the substrate materials used. Fig. 5 shows a typical set of measurements, starting from the AU5GT substrate side to the external surface of a coating of alloy A. The microhardness values are reported in the upper part of the figure. Micrography helps one to evaluate the quality of the present coating that was prepared by technique T. The porosity was evaluated with the help of a quantitative image analyser and is approximately 15%. This figure is significantly reduced, by at least a factor of two, when using technique S. Trials with a plasma spray method are in progress and this further improves the compactness of the coating.

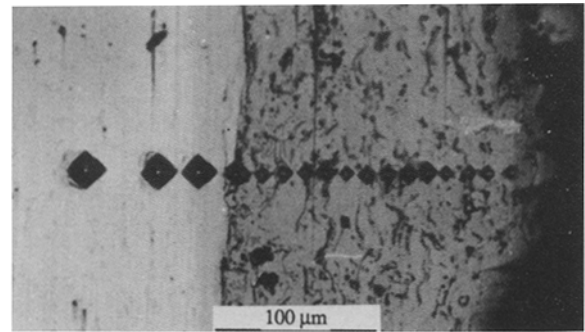
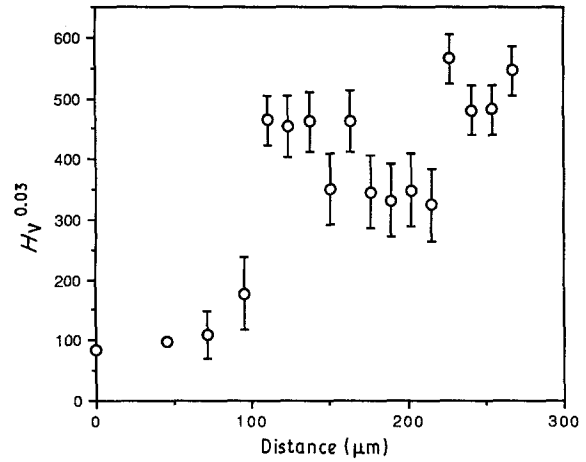


Figure 5 Microhardness  $H_V$  of an AU5GT substrate coated with alloy A.

The mechanical resistance of the substrate plus coating composite system has been assessed by means of a commercial scratch testing device equipped with acoustic emission (AE) and friction force ( $F_t$ ) sensors for on-line measurement. This test rig has been described elsewhere [21]. It is operated either with a Rockwell C diamond indenter (indenter D, cone angle: 120°, tip radius: 0.2 mm) or a Brinell ball (indenter B: AISi 52100 steel, radius: 0.79 mm). Two operation modes have been practiced:

(i) For *progressive loading* (indenter D only) the normal load  $F_N$  on the coated surface is increased linearly with sliding (scratching) distance. Brittle surface damage is detected by means of AE bursts. In the case of cohesive spalling of coating fragments strong oscillations in  $F_t$  are monitored. Coating perforation and/or adhesive failure result in a steep increase in AE and a change of the friction coefficient  $\mu = F_t/F_N$  (slope of the  $F_t-F_N$  plot). The corresponding critical normal load for coating perforation  $F_N^c$  is also verified by means of post-test SEM or reflected-light microscopy.

(ii) Under *constant loading* the indenter is drawn over the coating under a constant normal load  $F_N < F_N^c$ . This operation is chosen for statistically reliable measurements of  $\mu$ . The results are reported in Table I for the substrates and Table II for the coatings.

Fig. 6a and b show the  $F_t$  and AE plots, respectively, against  $F_N$  under progressive loading of the diamond indenter. They give clear evidence of coating perforation at  $F_N^c$  which is indicated by a

TABLE II Coatings

Coating No.	Alloy	Substrate	Spraying technique	Thickness ( $\mu\text{m}$ )	Hardness $H_V^{\text{D}} \pm 50$	$\mu^*$	
						Indenter D	Indenter B
1	A	b	S	$125 \pm 15$	540	0.193	
2	A	b	S	$320 \pm 15$	540	0.196	0.224
3	A	b	S	$90 \pm 30$	540	0.256	
4	A	b	S	$75 \pm 25$	540	0.253	0.286
5	A	b	S	$60 \pm 30$	540	0.236	0.370
6	B	b	T	$35 \pm 10$	550	0.249	
7	B	c	T	$155 \pm 30$	550	0.218	0.323
8	B	a	T	$240 \pm 60$	550	0.216	0.305
9	B	a	T	$130 \pm 25$	550	0.271	0.344

\* The accuracy is estimated from at least two sets of three tests, each set being measured with a load  $F_N = 40 \text{ N}$ .

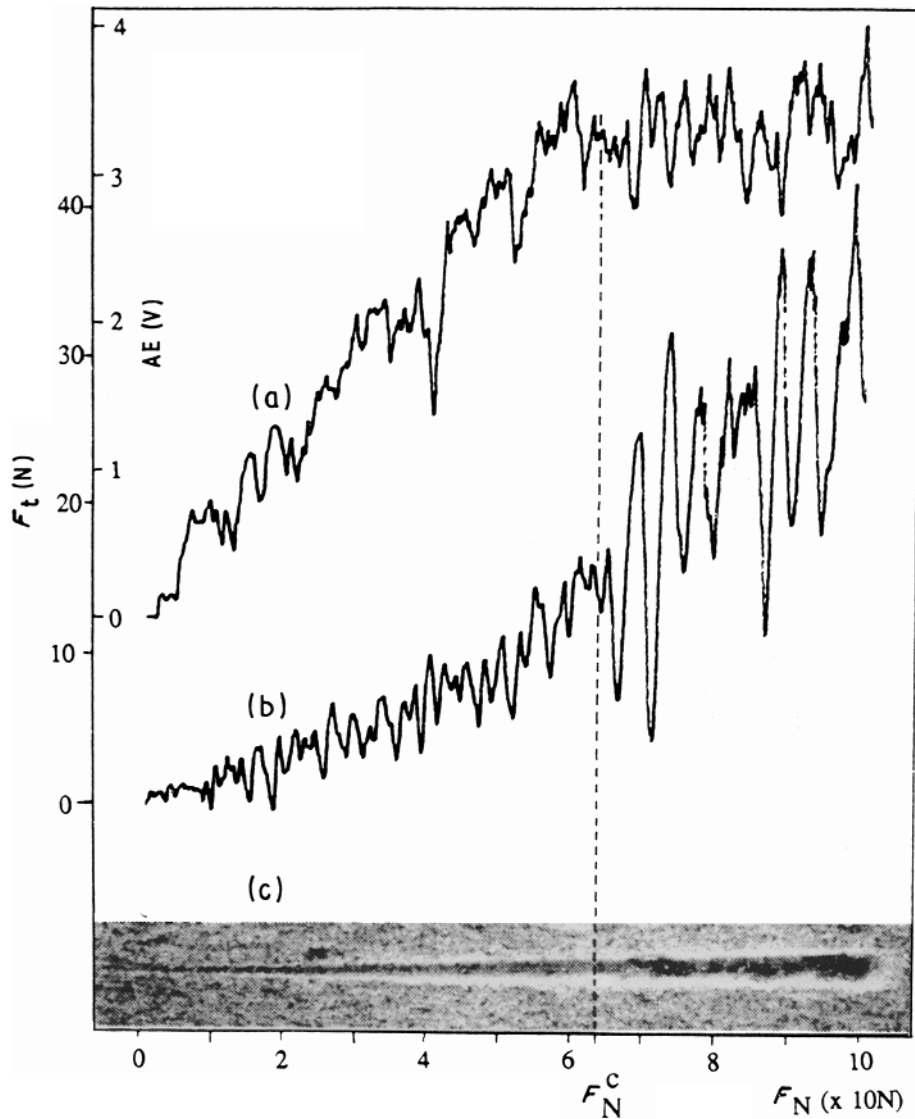


Figure 6 (a) Tangential force  $F_t$ , (b) acoustic emission (AE) and (c) micrography of a scratch as observed versus increasing load  $F_N$  in a coating of alloy A.

deeper rise in AE and as a increase in slope for  $F_t$  versus  $F_N$ , while the corresponding SEM micrograph (Fig. 6c) shows a continuous increase in the scratch track width even in the vicinity of the perforation load  $F_N^c$ . This is clear indication of essentially ductile deformation of the coating plus substrate composite. In particular it shows that there is no problem concerning coating-substrate adhesion.

In addition, Fig. 7 shows the linear increase of  $F_N^c$

with coating thickness. When assuming perfect coating-substrate interface adhesion this is expected, if under progressive loading the diamond scratch indenter ploughs deeper and deeper into a plastically deforming composite system until it reaches this very interface.

In conclusion, coatings containing a significant amount of quasicrystalline phases may offer an interesting alternative to the surface reinforcement of soft metallic materials. They are hard ( $H_V < 500$ )

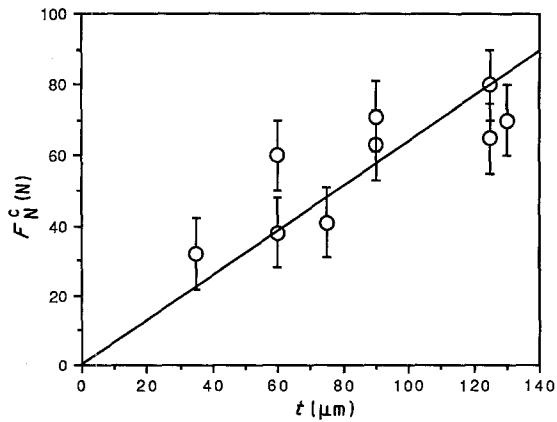


Figure 7 Critical load  $F_N^c$  versus thickness  $t$  of the coating.

and ductile. Their friction coefficient is less than half that of the aluminium-based substrates studied in the present paper and as good as that of a low-carbon steel. This point makes them good candidates for mild wear applications. Furthermore, they are thermally stable and their composition may be adjusted for the purpose of some corrosion-resistant applications.

### Acknowledgements

Grateful thanks are due to the Direction de la Valorisation (CNRS) and to the Association pour le Transfert de Technologie en Lorraine for their generous support of the present study. We are indebted to M. P. Weinland for his technical assistance and to Dr A. Pianelli for the provision of X-ray facilities.

### References

1. D. SCHECHTMAN, I. BLECH, D. GRATIAS and J. CAHN, *Phys. Rev. Lett* **53** (1984) 1951.

2. C. JANOT and J. M. DUBOIS, *J. Phys. F: Met. Phys.* **18** (1988) 2303.
3. P. J. STEINHART and S. OSTLUND, "The Physics of Quasicrystals" (World Scientific, Singapore, 1987).
4. C. JANOT, J. PANNETIER, J. M. DUBOIS and M. de BOISSIEU, *Phys. Rev. Lett.* **62** (1989) 450.
5. L. BENDERSKY, *ibid.* **55** (1985) 1461.
6. B. DUBOST, J. M. LANG, M. TANAKA, P. SAINFORT and M. AUDIER, *Nature* **324** (1986) 48.
7. A. P. TSAI, A. INOUE and T. MASUMOTO, *Jap. J. Appl. Phys.* **26** (1987) L1505.
8. K. H. KUO, in Proceedings of Adriatic Research Conference on Quasicrystals, Trieste, July 1989, edited by M. Jaric (World Scientific, Singapore, in press) p. 92.
9. M. AUDIER and P. GUYOT, in Proceedings of 3rd International Workshop on Quasicrystals, Mexico, 1989, in press p. 288.
10. C. DONG and J. M. DUBOIS, *J. Mater. Sci.* submitted.
11. J. L. VERGER-GAUGRY, *J. Phys. (Paris)* **49** (1988) 1867.
12. M. AUDIER, M. de BOISSIEU, J. M. DUBOIS and C. JANOT, *Phys. Rev. Lett.* submitted.
13. P. SAINTFORT and B. DUBOST, in "Quasicrystalline Materials", edited by C. Janot and J. M. Dubois (World Scientific, Singapore, 1988) p. 361.
14. H. SIDHOM and R. PORTIER, *Phil. Mag. Lett.* **59** (1989) 131.
15. L. Y. YANG, *J. Phys. F: Met. Phys.* **17** (1987) L97.
16. P. J. BLACK, *Acta Crystallogr.* **8** (1955) 43.
17. P. RAMACHANDRARAO and M. LARIDJANI, *J. Mater. Sci.* **9** (1974) 434.
18. M. G. BROWN and P. J. BROWN, *Acta Crystallogr.* **9** (1956) 911.
19. J. W. CAHN, D. SHECHTMAN and D. GRATIAS, *J. Mater. Res.* **1** (1986) 13.
20. A. YAMAMOTO and K. N. ISHIHARA, *Acta Crystallogr.* **A44** (1988) 707.
21. J. von STEBUT, in Proceedings of First International Conference on Plasma Surface Engineering, Garmish-Partenkirchen, 1988) p. 1.

Received 2 March  
and accepted 27 June 1990